Supplementary Information for

"An environmental determinant of viral respiratory disease"

Yeon-Woo Choi[1,†], Alexandre Tuel[1,†,*], and Elfatih A. B. Eltahir[1]

May 27, 2020

[1]Ralph M. Parsons Laboratory, Massachusetts Institute of Technology, Cambridge, Massachusetts 02139, USA

* e-mail: atuel@mit.edu

† equal contribution

Contents

Supplementary Methods

Maxwell theory and derivation of ADC.

We derive equations for the rate of change in the radius of a spherical liquid water droplet under given ambient temperature and relative humidity. Further details can be found in Rogers and Yau[33]. When ambient conditions are different from those prevailing near the surface of the droplet, heat and mass transfers occur that drive droplet growth and decay. We assume steady-state and isotropic conditions for ambient water vapour ρ_a and temperature T_a:

$$\nabla^2 \rho_a = 0, \quad \nabla^2 T_a = 0 \quad (1)$$

Denoting by ρ_s the water vapour concentration near the surface of the droplet, the mass balance of the droplet is given by

$$\frac{dm}{dt} = 4\pi r D(\rho_a - \rho_s) \quad (2)$$

with m the mass of the droplet, r its radius and D the diffusion coefficient of water vapor. The condensation/evaporation associated with this mass transfer releases latent heat. Additionally, differences in temperature between the ambient value T_a and that at the surface of the droplet T_s lead to heat transfer given by:

$$\frac{dQ}{dt} = 4\pi r K(T_s - T_a) \quad (3)$$

where Q is heat and K the thermal conductivity of air. Accordingly, the change in droplet surface temperature is determined by heat transfer and latent heat release:

$$\frac{4}{3}\pi r^3 \rho_w c_w \frac{\mathrm{d}T_s}{\mathrm{dt}} = L_v \frac{dm}{dt} - \frac{dQ}{dt} \quad (4)$$

where ρ_w and c_w are the density and specific heat capacity of water, respectively, and L_v is the latent heat of vaporisation. Assuming steady-state conditions, $\frac{dT_s}{dt} = 0$ which yields:

$$L_v \frac{dm}{dt} = \frac{dQ}{dt} \quad (5)$$

By inserting (2) and (3) in (5), we get:

$$\frac{\rho_a - \rho_s}{T_s - T_a} = \frac{K}{L_v D} \quad (6)$$

In (6), ρ_a and T_a are given, and the right-hand side is a function of ambient temperature and pressure only. ρ_s can be approximated using the equation of state for water vapour, and an empirical approximation involving the effects of surface tension and solute concentration in the droplet:

$$\rho_s = \left(1 + \frac{a}{r} - \frac{b}{r^3}\right) \frac{e_s(T_s)}{R_v T_s} \quad (7)$$

where $e_s(T_s)$ is the saturation vapour pressure at temperature T_s given by the Clausius-Clapeyron equation and R_v is the specific gas constant for water vapor. $a = \frac{2\sigma}{\rho_w R_v T_s}$ and $b = 8.6\frac{M}{m_s}$ are coefficients accounting for surface tension and solute concentration, respectively, for surface tension σ, a mass M of diluted solid, of molar mass m_s The closed system (6-7) can be solved analytically by applying one last approximation to relate changes in saturated vapour density to changes in temperature:

$$\frac{\rho_a^{sat} - \rho_s^{sat}}{\rho_s^{sat}} \approx \frac{T_a - T_s}{T_a} \left(\frac{L_v}{R_v T_a} - 1\right) \quad (8)$$

This yields in the end the following expression for the rate of droplet growth:

$$r\frac{dr}{dt} = \frac{(RH-1) - \frac{a}{r} + \frac{b}{r^3}}{(\frac{L_v}{R_v T_a} - 1)\frac{L_v \rho_a}{KT} + \frac{\rho_a R_v T_a}{e_s(T_a) D})} \quad (9)$$

where $RH = \rho_a / \rho_a^{sat}$ is the ambient relative humidity. The effects of radius and solute concentration can be neglected for droplets of typical range (>1μm) but are included when solving (9) in practice. K and D are also functions of air temperature and droplet velocity, for which simple formulations can be used[33].

Equations of motion of airborne free-falling droplets.

To solve for the radius of droplets in motion, (9) must be supplemented by the equation of motion for a single droplet of mass m, radius r and vertical velocity v (negative for downward motion):

$$m\frac{dv}{dt} = -mg - \frac{\pi r^2 C_d \rho_g}{2}|v|v \quad (10)$$

where g is gravitational acceleration, ρ_g the density of air and C_d the drag coefficient. As in Xie et al.[12], we model C_d as a function of droplet Reynolds number $\mathrm{Re} = \frac{\rho_g r v}{\mu}$ (μ is dynamic viscosity of air) by

$$C_d = \begin{cases} 0.424 & \mathrm{Re} > 1000 \\ \frac{24}{\mathrm{Re}}\left(1 + \frac{1}{6}\mathrm{Re}^{2/3}\right) & \mathrm{Re} \leq 1000 \end{cases}$$

The diffusion coefficient D and thermal conductivity of air K are also dependent on droplet velocity (heat and mass transfer are enhanced at higher velocity) and are replaced in (9) by D^*, K^* as follows[12]:

$$\begin{cases} D^* = D \cdot (1 + 0.3 \cdot \mathrm{Re}^{1/2} \cdot \mathrm{Sc}^{2/3}) \\ K^* = D \cdot (1 + 0.3 \cdot \mathrm{Re}^{1/2} \cdot \mathrm{Pr}^{1/3}) \end{cases}$$

where Sc is the Schmidt number and Pr the Prandtl number. Finally, to estimate b in (9), we assume that only NaCl is diluted in the droplet, with a concentration of 0.1mol/m^3 [37], or roughly 6g/l.

Influenza prevalence indices.

It is not straightforward to determine an index of influenza incidence from the WHO FluNet dataset. Variations in the number of subjects tested every week, both within each country and between countries, introduce a sampling bias, in addition to a reporting bias due to uneven reporting frequencies across countries. Richer mid-latitude countries, where influenza is more common, tend to test more than warm, tropical countries with less incidence of influenza. Similarly, countries where influenza is more widespread will tend to test more people. We address the bias in sampling by introducing an "influenza frequency index", defined weekly as the number of positive influenza A and B cases divided by the number of tested subjects. To partially correct for limited testing, we remove for each country the 10% of data points with the lowest testing numbers. This empirical frequency is not perfect, since some countries may prioritise symptomatic subjects for testing while others may test more systematically. However, it provides a first-order correction for testing rate between countries.

To tackle the bias in reporting, we adopt the approach of Deyle et al.[14] by defining for each country a weekly "normalized influenza prevalence (NIP)" index as the number of positive cases divided by population (linearly interpolated over time to account for population trends), and multiplied by the average number of annual reports for all countries divided by the average

number of annual reports for the country in question:

$$NIP(\mathrm{t}, \mathrm{C}) = \frac{\#\ \text{positives, country C, week t}}{\text{population, country C}} \times \frac{\text{avg \# weekly reports, all countries}}{\text{avg \# weekly reports, country C}}$$

This normalised index offers some idea of the overall incidence of influenza for a given country. Nevertheless, the NIP index is less robust to country-to-country comparisons than the frequency index defined above, due to wide variations in average testing numbers between countries.

Despite these shortcomings, our conclusions do not change by considering either index (Fig. 4-a,b). We also defined these indices based on monthly, monthly-mean and seasonal-mean data, and found no significant difference in the results.

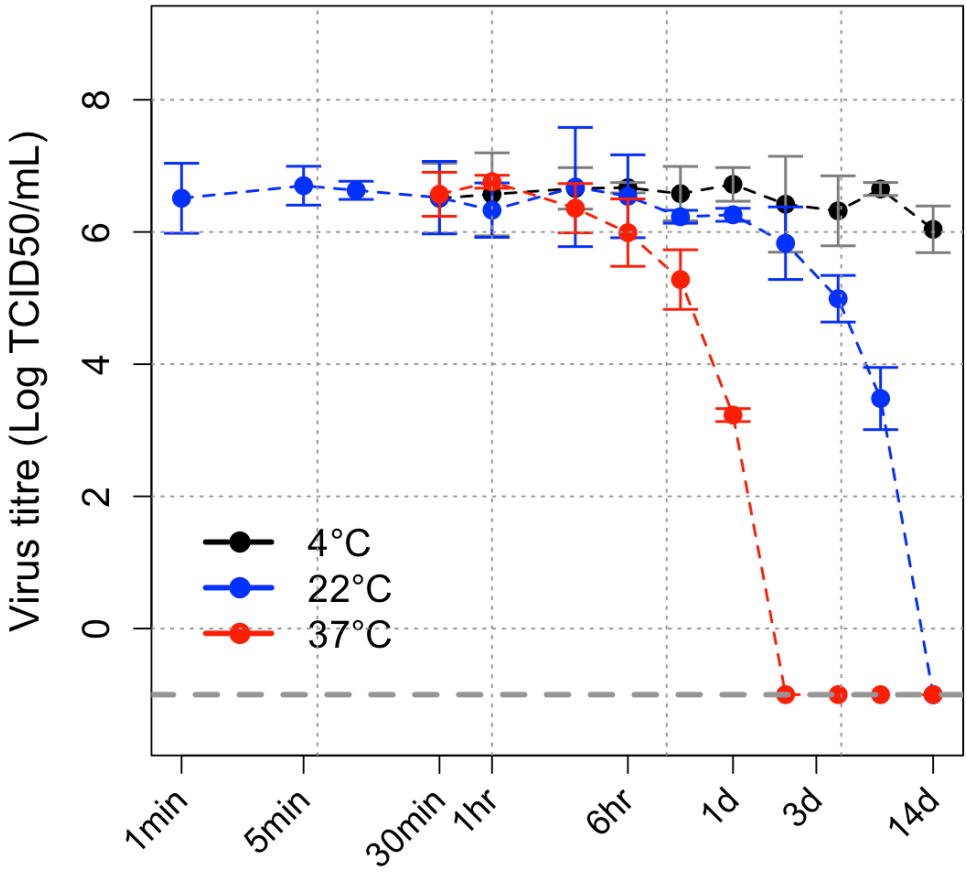

Figure S1: **SARS-CoV-2 resistance to temperature**. Virus titre as function of time under various temperature conditions. Data from Chin et al.[8].

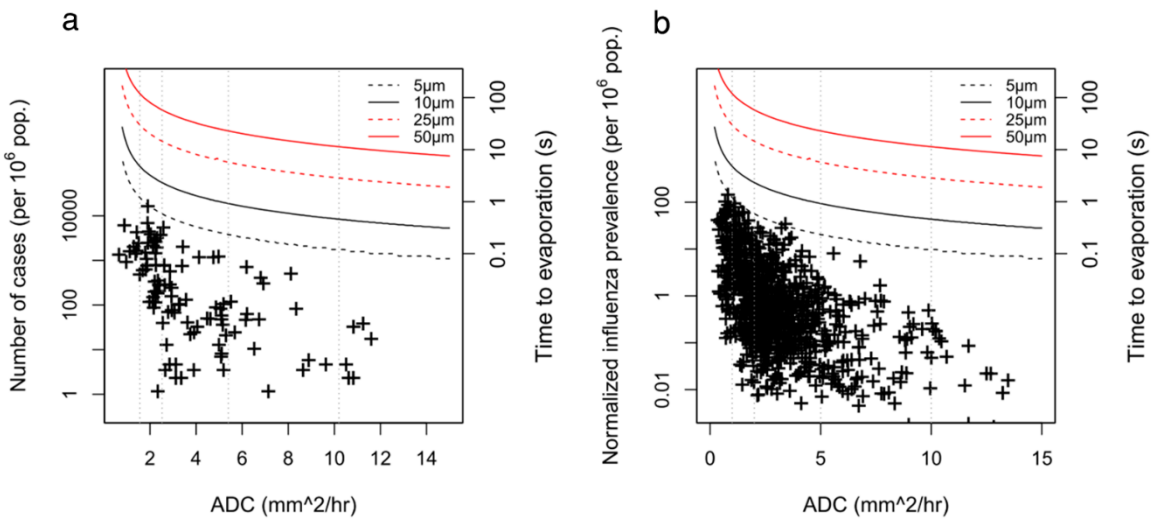

Figure S2: **Transmission of VRD and time to droplet evaporation**. (a) ADC against accumulated confirmed COVID-19 cases for 108 countries (Supplementary Table 1) from February to April 2020. (b) Long-term seasonal mean ADC against long-term seasonal mean normalized influenza type A and B prevalence for 85 countries (Supplementary Table 1) from October 1995 to August 2019. Contour lines in (a), (b) denote the time to evaporation of free-falling spherical droplets as a function of ADC for various initial droplet radii.

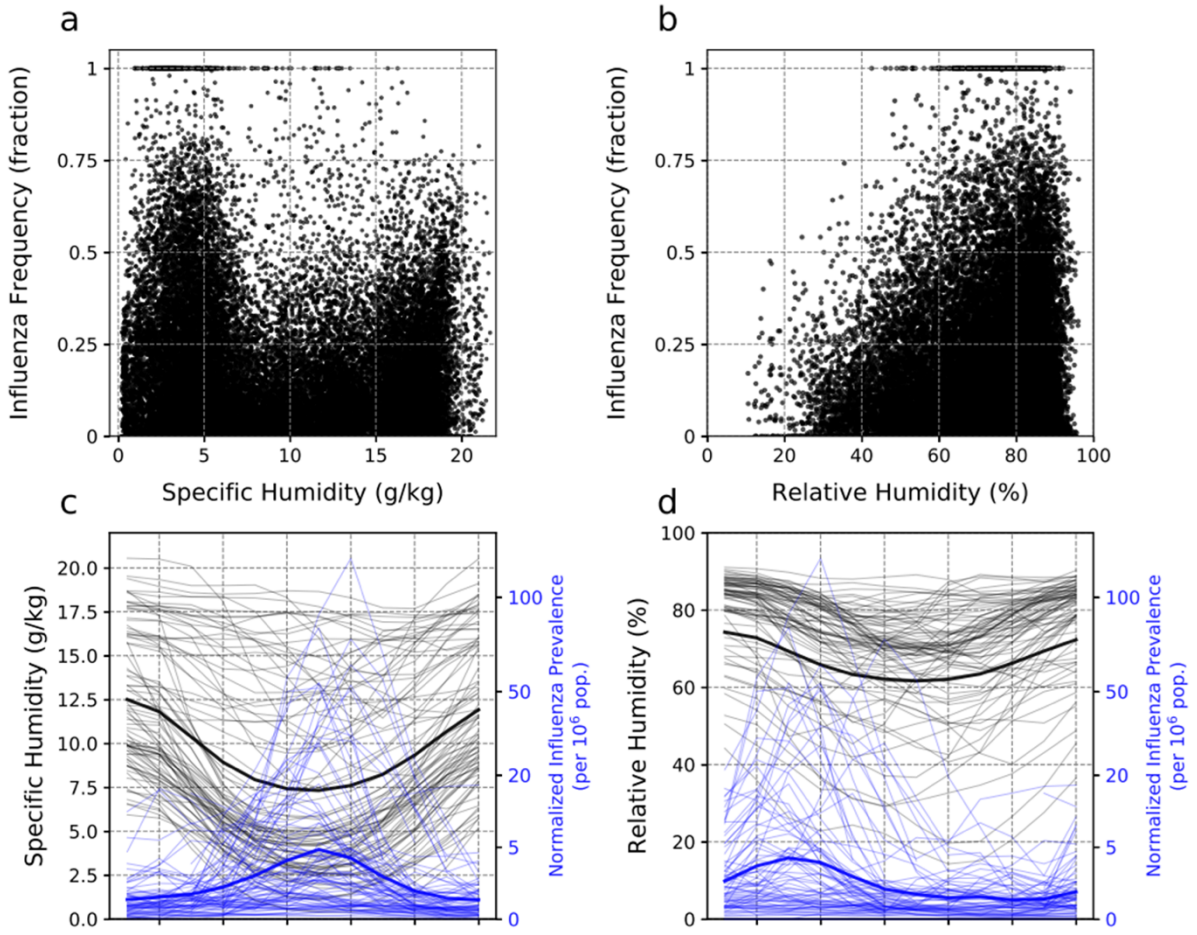

Figure S3: (a-b) Weekly influenza prevalence against (a) specific humidity and (b) relative humidity. (c-d) Seasonal variation of influenza prevalence alongside (c) specific humidity and (d) relative humidity. In (c-d), the first month is defined for each of the 85 countries as the month with maximum (c) specific humidity and (d) relative humidity.

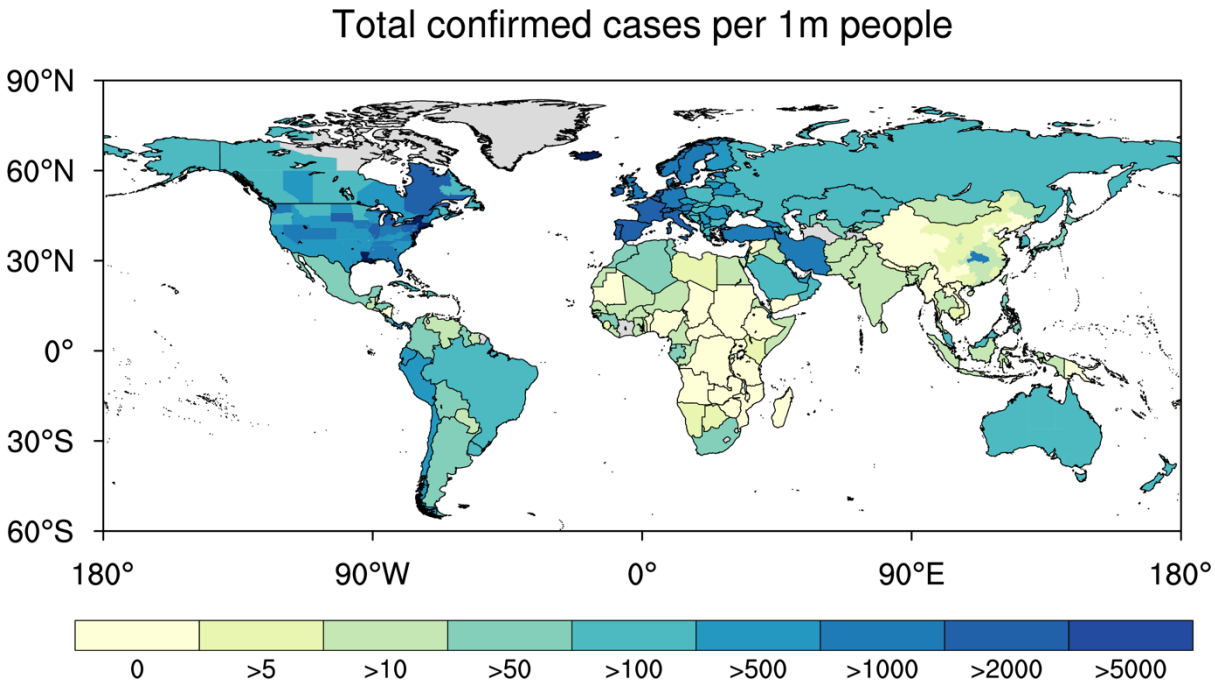

Figure S4: Global total confirmed COVID-19 cases per million people (accessed April 22th 2020; See Data). Missing values are depicted in grey color.

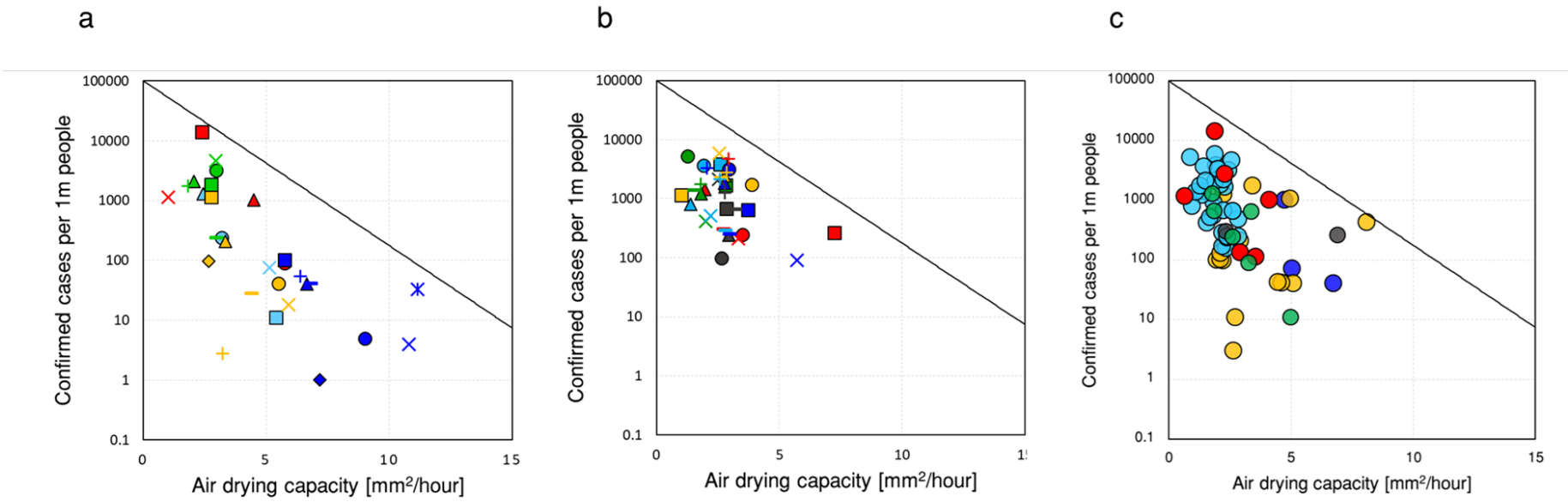

Figure S5: (a-b) February-April 2020 average ADC against concurrent accumulated confirmed COVID-19 cases for (a) 29 representative countries, (b) 36 OECD countries and (c) countries among the 108 from Fig. 4-c that tested at least 1000 people per million population. Colors correspond to each of the 6 continents: North America (red), South America (green), Africa (blue), Asia (yellow), Europe (light blue), and Oceania (black). The respective country lists are given in Table S1.

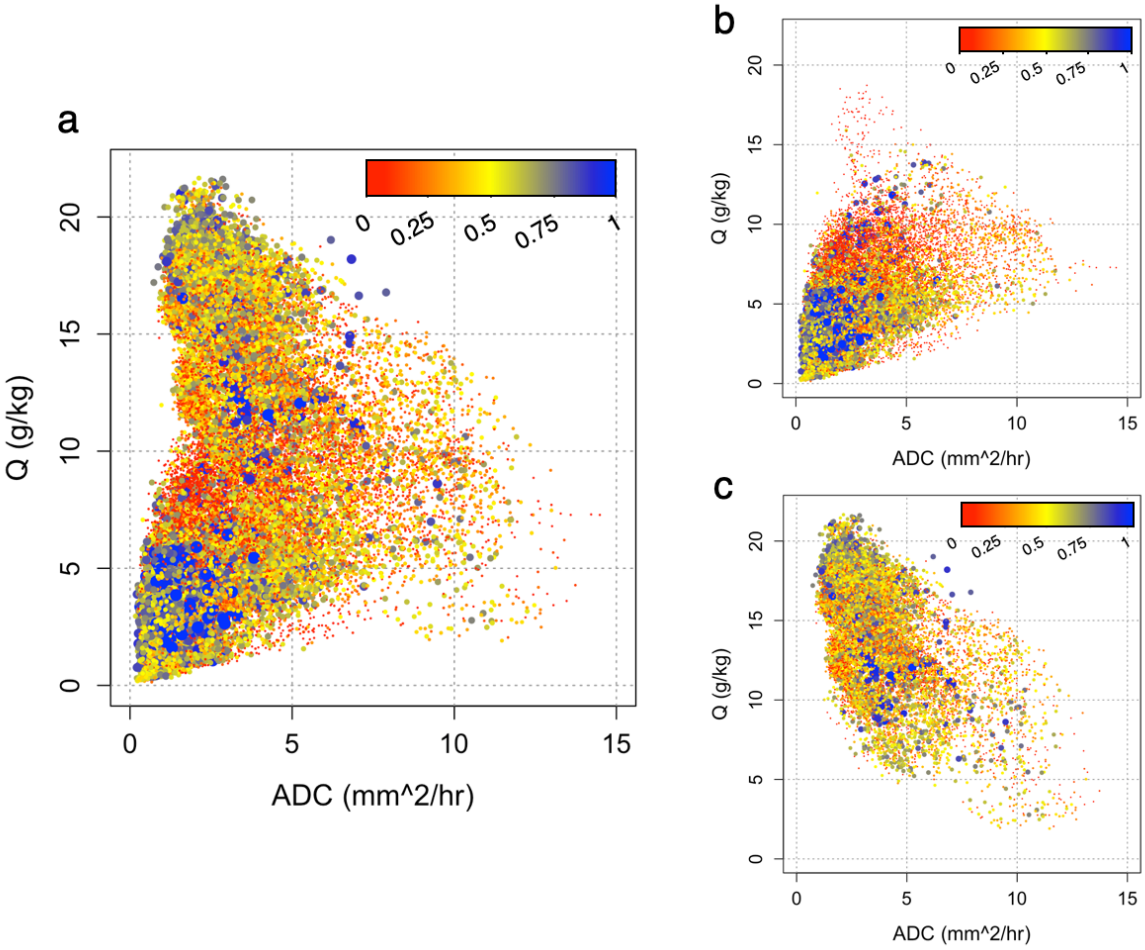

Figure S6: Weekly-mean ADC against specific humidity; with the color and size of dots corresponding to weekly influenza frequency (0: red, small dot; 1: blue, large dot), for (a) all 86 available countries, (b) mid-to-high latitude countries (poleward of 25°S/N) and (c) tropical countries (equatorward of 25°S/N).

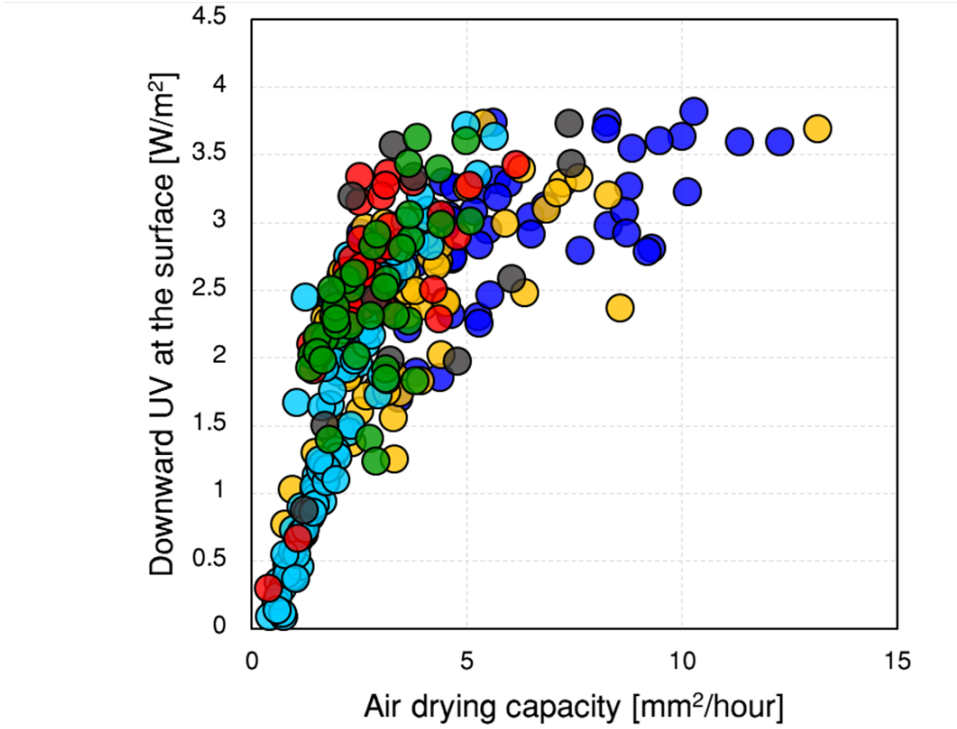

Figure S7: Seasonal mean ADC against seasonal mean surface downward UV for 85 countries (Table S1). Data is from ERA-Interim (1995-2014). Each country is represented by four seasonal values. Colors correspond to each of the 6 continents: North America (red), South America (green), Africa (blue), Asia (yellow), Europe (light blue), and Oceania (black).

	List of countries
85 countries (influenza analysis)	Argentina, Australia, Austria, Bangladesh, Belarus, Belgium, Brazil, Bulgaria, Cambodia, Cameroon, Canada, Chile, China, Colombia, Costa Rica, Croatia, Cuba, Czech Republic, Denmark, Dominican Republic, Ecuador, Egypt, El Salvador, Estonia, Ethiopia, Finland, France, French Guiana, Germany, Ghana, Greece, Honduras, Iceland, India, Indonesia, Iraq, Ireland, Israel, Italy, Jamaica, Japan, Kazakhstan, Kenya, Kyrgyzstan, Latvia, Luxembourg, Madagascar, Malaysia, Mexico, Mongolia, Morocco, Netherlands, New Caledonia, New Zealand, Niger, Nigeria, Norway, Pakistan, Panama, Paraguay, Peru, Philippines, Poland, Portugal, Romania, Senegal, Singapore, Slovakia, Slovenia, South Africa, South Korea, Spain, Sri Lanka, Sudan, Sweden, Switzerland, Thailand, Tunisia, Turkey, Uganda, Ukraine, United Kingdom, Uruguay, Vietnam, Venezuela
108 countries (COVID-19 analysis)	New York state, California, Afghanistan, Albania, Algeria, Angola, Argentina, Armenia, Australia, Austria, Azerbaijan, Bangladesh, Belarus, Belgium, Bolivia, Brazil, Bulgaria, Burma, Cambodia, Cameroon, Canada, Central African Republic, Chad, Chile, China, Colombia, Congo, Costa Rica, Croatia, Cuba, Cyprus, Czechia, D.R. Congo, Denmark, Djibouti, Ecuador, Egypt, Estonia, Ethiopia, Finland, France, Gabon, Gambia, Germany, Ghana, Greece, Guatemala, Hubei, Hungary, Iceland, India, Iran, Iraq, Ireland, Israel, Italy, Jamaica, Japan, Jordan, Kazakhstan, Kenya, Kuwait, Kyrgyzstan, Laos, Latvia, Lebanon, Libya, Lithuania, Luxembourg, Madagascar, Malaysia, Mali, Mauritania, Mexico, Mongolia, Morocco, Mozambique, Nepal, Netherlands, New Zealand, Niger, Nigeria, Norway, Oman, Pakistan, Paraguay, Peru, Philippines, Poland, Portugal, Saudi Arabia, Senegal, Slovakia, Slovenia, Somalia, South Africa, South Korea, Spain, Sri Lanka, Sudan, Sweden, Thailand, United Kingdom, United States, Venezuela, Vietnam, Switzerland, Turkey
29 countries (Fig. S5-a)	New York, California, Mexico, Canada, Venezuela, Ecuador, Brazil, Argentina, Morocco, Ethiopia, Egypt, Nigeria, Sudan, Ghana, Cameroon, Senegal, Hubei, Japan, South Korea,

	Thailand, India, Bangladesh, Vietnam, Germany, United Kingdom, Italy, Spain, Greece, Sweden
36 OECD countries (Fig. S5-b)	Australia, Austria, Belgium, Canada, Chile, Czech Republic, Denmark, Estonia, Finland, France, Germany, Greece, Hungary, Iceland, Ireland, Israel, Italy, Japan, South Korea, Latvia, Lithuania, Luxembourg, Mexico, Netherlands, New Zealand, Norway, Poland, Portugal, Slovakia, Slovenia, Spain, Sweden, Switzerland, Turkey, United Kingdom, United States.
65 countries (Fig S5-c)	Iceland, Luxembourg, New York state, Cyprus, Estonia, Lithuania, Israel, Portugal, Norway, Switzerland, Italy, Germany, Austria, Latvia, Ireland, New Zealand, Slovenia, Denmark, Spain, Czechia, Australia, Canada, Belgium, Venezuela, Belarus, Finland, California, South Korea, Azerbaijan, Djibouti, Slovakia, Netherlands, Turkey, Sweden, UK, Kazakhstan, Chile, Croatia, France, Poland, Kyrgyzstan, Jordan, Hungary, Peru, Greece, Saudi Arabia, Armenia, Iran, Bulgaria, Malaysia, Lebanon, Ecuador, Cuba, Ghana, South Africa, Costa Rica, Albania, Mongolia, Vietnam, Thailand, Iraq, Colombia, Brazil, Japan

Table S1: List of countries used in this study. 85 countries used for Figures 3, 4-a,b, S2, S3 are selected based on the availability of influenza data retrieved from the WHO's FluNet database. 108 countries used for Figure 4-c is selected based on the available COVID-19 data. 29 countries used for Figure S5-a are selected to be representative of the equal representation for ADC values.